AIAA 81-2031R

Rotor Wake Characteristics Relevant to Rotor-Stator Interaction Noise Generation

Loretta M. Shaw* and Joseph R. Balombin†
NASA Lewis Research Center, Cleveland, Ohio

Mean and turbulence wake properties at three axial locations behind the rotor of an aerodynamically loaded 1.2 pressure ratio fan were measured using a stationary cross-film anemometer in an anechoic wind tunnel. Wake characteristics at four radial immersions across the duct at four different fan speeds were determined utilizing a signal enhancement technique. The shapes of the waveforms of the mean rotor relative and mean upwash velocities were shown to change significantly across the span of the blades. In addition, an increase in fan rotational speed caused an increase in the maximum wake turbulence intensity levels near the hub and tip. Spectral analysis was used to describe the complex nature of the rotor wake.

Introduction

ONE of the major contributions to the overall noise production by turbofans is rotor-stator interaction. One cause of this interaction noise is the fluctuating lift forces acting on the stator vanes as a result of the rotor wakes or tip vortices interacting with the stator.[1,2] The purpose of the present investigation is to experimentally study the variation of the mean and fluctuating properties of rotor wakes across the duct of an aerodynamically loaded 0.5-m-diam fan. The data resulting from this study could then be correlated with acoustic measurements[3] and be used as input for sound generation theoretical models.

A previous paper by Shaw and Glaser[4] reviewed experiments of other investigators and presented mean rotor wake properties in the tip and midspan region behind the rotor blades in a stationary reference frame. In the present study, mean and turbulence properties of the rotor wakes in both the stationary and the rotor relative coordinate system were investigated at three axial stations downstream from the fan.

The present experimental program was part of a larger fan noise program in which fan noise characteristics were determined as a function of rotor-stator spacing, rotor and stator blade number, and with and without the effects of forward velocity. The experiments were conducted in the NASA Lewis 9×15-ft low-speed anechoic wind tunnel. The fan stage studied had 15 rotor blades, a design pressure ratio of about 1.2 at a tip speed of 213 m/s (700 ft/s). Wake characteristics were measured with a cross-film anemometer oriented to sense the streamwise and upwash components of the rotor wakes. The wakes were measured at downstream distances of 0.54, 1.23, and 1.77 mean-radius aerodynamic rotor chords. In axially projected rotor chords, the downstream distances were from 0.59 to 1.94 chords. This spacing range was selected to ensure that rotor-stator noise would be the dominant source in the experiment.

The data were analyzed to yield the magnitude and width of the wake defect of both the total relative velocity and the upwash velocity component. A comparison of the decay of the velocity defect of the rotor relative velocity with empirical correlations and data from previous investigators is made. The effects of radial immersion, forward velocity, and downstream distance on the turbulence levels in the wake are also examined. Finally, a spectral analysis of the waveforms of the relative velocity and upwash velocity component is performed to yield the amplitude of the spatial harmonics of the wakes. In this form, the data should be useful as input to models of fan noise generation.

Presented as Paper 81-2031 at the AIAA 7th Aeroacoustics Conference, Palo Alto, Calif., Oct. 5-7, 1981; submitted Oct. 26, 1981; revision received Feb. 26, 1982. This paper is declared a work of the U.S. Government and therefore is in the public domain.

*Aerospace Engineer. Member AIAA.
†Aerospace Engineer.

Apparatus and Procedure

Experimental Test Facility

The NASA Lewis 9×15-ft anechoic wind tunnel is located in the return loop of the 8×6-ft supersonic tunnel. The aerodynamic and acoustic properties of the low-speed section are documented in Refs. 5 and 6. The airflow in the test section is varied by control of both the tunnel drive motor speed and the position of the control doors located immediately upstream of the test section. The tunnel was operated both statically and with a freestream velocity of 41 m/s.

Fan and Installation

The 50.8-cm-diam fan has 15 blades and 25 vanes. The vanes were positioned at three different mean-radius rotor blade chord spacings: 0.54, 1.23, and 1.77 chords. The spacings were based on a 7.7-cm midspan aerodynamic rotor chord. The fan design pressure ratio and work coefficient (change in tangential velocity normalized by tip speed) were 1.2 and 0.43, respectively. The aerodynamic performance of the fan is documented in Ref. 8.

A conventional low throat Mach number (0.60) flight inlet was used for the tests. The 1.46 contraction ratio inlet had a 2:1 elliptically contoured lip and a length of approximately 52.6 cm. Aerodynamic performance of the inlet can be found in Ref. 8. The installation of the fan in the wind tunnel is shown in Fig. 1. Shown in the photograph is a rotating microphone boom along with several aft microphones. The acoustic data from these microphones are not presented in this paper, but are reported in Ref. 3.

Instrumentation and Procedure

Rotor wake properties were measured with a cross-film anemometer. Each film was 70 μm in diameter and 1.25 mm long. The cross-film anemometer was located in the plane of the leading edge of the stator vanes midway between two vanes (Fig. 2) except for one series of experiments. In that series, the anemometer was located midway between two vanes but upstream of the stator leading-edge plane. Since the

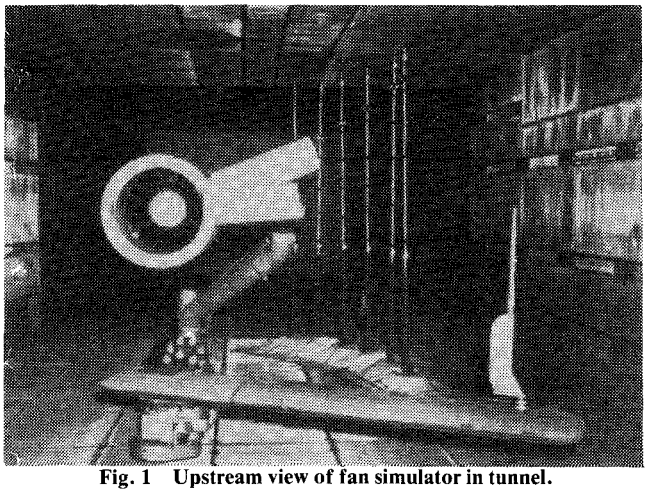

Fig. 1 Upstream view of fan simulator in tunnel.

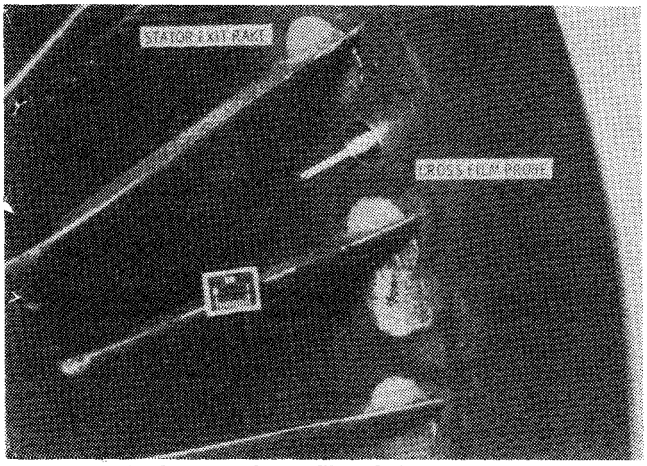

Fig. 2 Position of cross film relative to stator vanes.

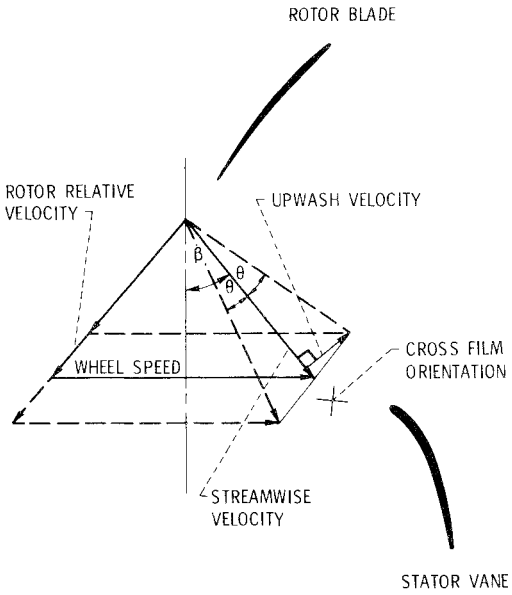

Fig. 3 Schematic of cross-film orientation (β = probe set angle, θ = fluctuating angle about β).

measurements were all midway between vanes even when in the plane of the stator leading edge, any effect due to the proximity of the stators was expected to be small.

Table 1 lists the axial spacings of the anemometer and stator vanes from the rotor blades for each test condition.

Table 1 Axial spacing of anemometers and stator vanes from motor blades

Test series	Rotor-stator spacing, rotor chords	Rotor-anemometer spacing, rotor chords
1	0.54	0.54
2	1.77	1.23
3	1.77	1.77

Figure 3 shows schematically the film orientation and the fluctuating velocity across a wake behind a rotor blade as it appears to a stator vane. Table 2 lists typical values of the streamwise Mach number measured by the cross-film probe and the probe set angles at 80% of design speed.

The streamwise velocity changes magnitude as it fluctuates between the angles $\beta \pm \theta$. The cross film was oriented so that the mean streamwise velocity component into the stator would bisect the angles formed by the two films. The cross film had been calibrated for yaw angle before the test so that the fluctuating angle (θ) would be measured accurately. The orientation of the cross film was such that both the streamwise and upwash components of the flow entering the stator row were determined. The upwash velocity component is normal to the streamwise velocity component shown in Fig. 3.

Measurements were made at several radial positions ranging from 9% of the span from the tip to 80% of the span. Data near the blade tip at 9% of the span from the tip (1.27 cm immersion) and at 30% of the span (4.05 cm immersion) at 80% design rpm are highlighted in this paper. The anemometer signals were linearized, summed and differenced, and dc suppressed before being recorded on magnetic tape. After linearization, the signals were digitized and analyzed with a computer program which utilized an ensemble averaging technique and Fourier transform analysis. Data averaging was done over 500 revolutions of the rotor and was triggered by a once-per-revolution signal generated by a magnetic pickup located on the rotor shaft and recorded on the data tape. Included in the program output were averaged waveforms through the wake, intensity levels, and spectra of the upwash component and relative velocity.

Results and Discussion

The wake data were analyzed in terms of mean and turbulence properties and harmonic content. The differences in wake properties between a near tip probe radial immersion and an immersion of 30% of the span from the tip are emphasized. The effects of forward velocity and fan speed on the wake properties are also examined. A comparison of measured mean wake parameters with empirical correlations and data of other experiments is presented. As was pointed out in the Apparatus and Procedure section, the data at 1.23 chords was obtained with the stator located at 1.77 chords, whereas the remaining data were obtained in the plane of the stator leading edge.

Wake Mean Properties

Figure 4 shows the mean rotor wake waveforms of the relative and upwash components of velocity across the span of the rotor blades at a rotor anemometer axial spacing of 1.23 rotor chords at 80% of design rpm with a tunnel velocity of 41 m/s. Away from the tip, the velocity waveforms are similar in shape with a single velocity defect region behind each blade. From Fig. 4 it can be seen that the defect varies in its width and amplitude as a function of position along the span. The majority of the waveforms are asymmetric but similar from blade to blade at 80% design speed. However, near the blade tip at a probe immersion of 9% of the span, the waveforms are characterized by two regions of velocity change behind each blade. The complex nature of the tip waveforms reflects the complicated flow pattern in the blade tip region. The

simple wakes and potential flows are complicated by interactions with the casing boundary flow as well as a number of secondary flows, for example, tip clearance flow, passage vortex flow, scraping vortex flow, etc. Some of these secondary flows are discussed by Dittmar,[2] Phillips and Head,[9] and Lakshminarayana and Ravindranath.[10] A tip vortex can be generated because of the clearance between the blade and the outer wall which allows communication between the pressure and suction sides of the blade, thus resulting in a secondary flow. It could also be generated by the relative motion of the blade scraping the wall boundary layer and rolling it into a vortex. Since the radial component of the velocity field behind the blade was not measured, it is not possible to determine which region of the tip waveforms shown in Fig. 4 can be attributed to a tip vortex.

The effects of tip speed on the change in mean velocity in the wake at the closest rotor stator spacing are shown in Fig. 5. In order to display the rotor wake behavior, a wake magnitude parameter, $\Delta V_w / V_{\text{freestream}}$, where ΔV_w is the peak-to-peak value of velocity in the wake and $V_{\text{freestream}}$ is the mean velocity outside of the wake, was defined. For the upwash component, ΔV_w is normalized by the freestream value of the absolute streamwise velocity component, while ΔV_w for the relative velocity is normalized by the rotor relative freestream velocity. In the near tip region, the effects of fan speed are minimal. At probe immersions from near tip to midspan, the rotor relative velocity defects decrease with increasing fan speed. This trend is consistent with that observed by Lakshminarayana et al.[11] Near the hub, however, both the rotor relative and the upwash velocity magnitudes show an increase with fan speed. The high levels of the wake magnitude parameter near the hub and tip reflect the large aerodynamic losses that occur in these regions.

For noise generation and other purposes, such as forced vibrations, one is interested in the decay characteristics of the wake as a function of downstream distance. Figures 6 and 7 examine the effects of rotor-stator spacing on the rotor wake magnitude parameter. To illustrate the effects of inflow turbulence and disturbances on the rotor mean properties, the wake magnitude parameter at 80% of design rpm is presented in Fig. 6 for a static tunnel flow condition ($U=0$) and a forward velocity condition ($U=41$ m/s). Forward velocity reduces the turbulence and other inflow disturbances entering the inlet by reducing the stream tube contraction ratio and eliminating many sources of flow disturbances associated with the flow being drawn over the cowl and support structure from the aft direction. This "cleanup" of the inflow greatly reduced the noise generated by the fan due to the rotor interaction with inflow disturbances.[12,13] The effects of freestream turbulence on rotor wake properties were systematically studied by Hah and Lakshminarayana.[14] They found that a large reduction in inflow turbulence intensity resulted in a minimal change in the velocity defect.

Figure 6 presents the effects of downstream distance and forward velocity on the relative velocity and upwash velocity component at a probe immersion of 30% of the span from the tip. The wake magnitude parameter ($\Delta V_w / V_{\text{freestream}}$) for both velocity components decays with increasing downstream distance. The magnitude of the upwash component decays at a faster rate than that of the rotor relative velocity, but both velocities reach the same value at the farthest rotor stator spacing. Forward velocity lowers the upwash parameter at the close rotor-stator spacing but has a minimal effect on the rotor relative velocity.

As discussed earlier, the tip rotor wake waveforms have a more complex shape than those at the other span positions. The schematics in Fig. 7 show that near the tip, the rotor wake waveform is characterized by two regions of velocity change behind each blade. Since one value of the wake magnitude parameter is not an adequate description of the dual change in velocity indicated by the waveforms, two values of the wake magnitude parameter are presented for each waveform—one describing the change in velocity on the pressure side of the waveform and one for suction side (see schematic in Fig. 7).

Table 2 Measured streamwise Mach numbers and probe set angles

Immersion, cm	Streamwise Mach no.	Probe set angle, deg
1.27	0.35	28.9
4.05	0.39	31.4

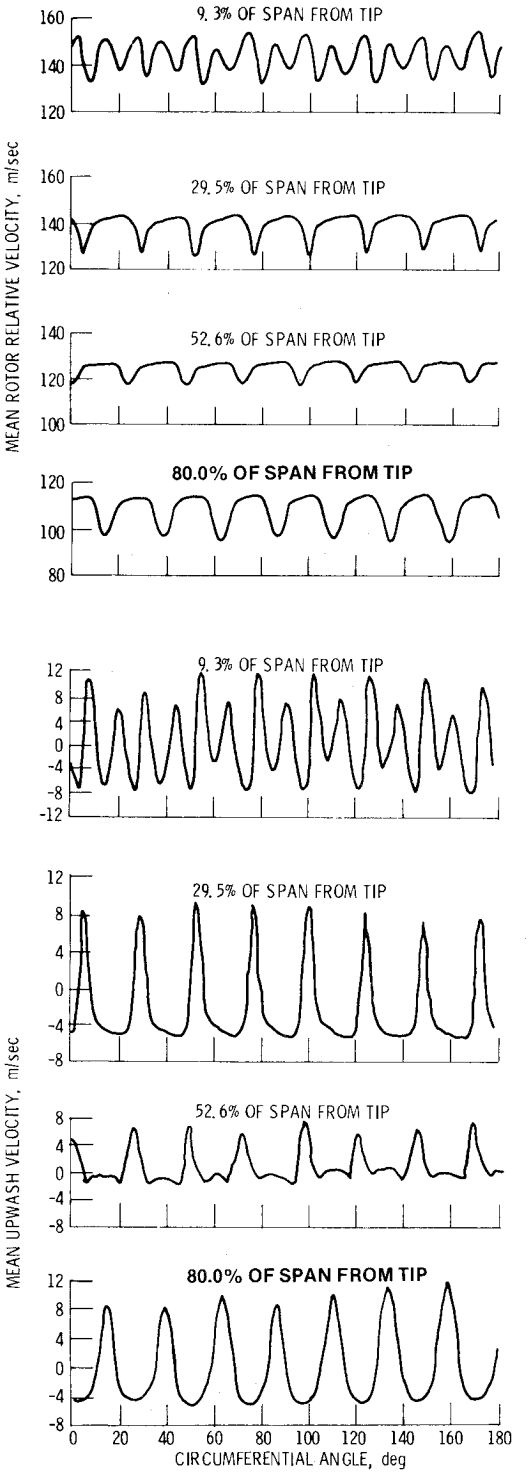

Fig. 4 Mean velocity across the duct at 80% of design rpm, 1.23 chord spacing, $U=41$ m/s. a) Rotor relative velocity; b) upwash component.

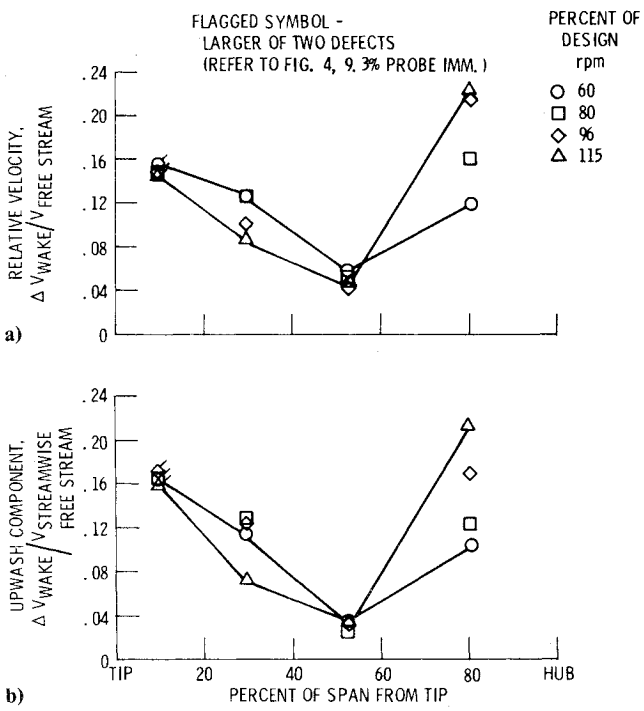

Fig. 5 Radial variation of the change in the mean velocity in the wake, 0.54 chord spacing, $U = 41$ m/s. a) Rotor relative velocity; b) upwash component.

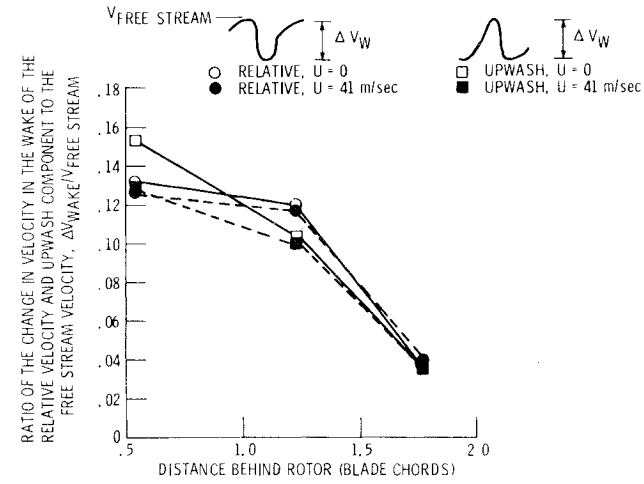

Fig. 6 Effect of downstream distance and forward velocity on the change in the relative velocity and upwash component in the wake at 30% of span from the tip, 80% of design rpm.

The wake magnitude on the pressure side of the waveform decays at a much faster rate than that on the suction side for both the relative velocity and upwash component. Between the first two downstream measuring stations, the magnitude of the upwash decays faster with forward velocity than with static tunnel operation.

Near the tip, the wake magnitudes at 115% of design speed are close to the same values as those at the lower fan speed of 80% rpm (Fig. 7c). Only one wake parameter for each waveform is plotted because the two regions of velocity change in each waveform now have merged to form one wide region of velocity change behind the rotor as shown in the schematic of Fig. 7c. The values of the wake magnitude parameter for the upwash component are higher than those of the relative velocity for the first two rotor anemometer spacings. However, at the farthest downstream spacings, the wake magnitudes for both velocities are the same.

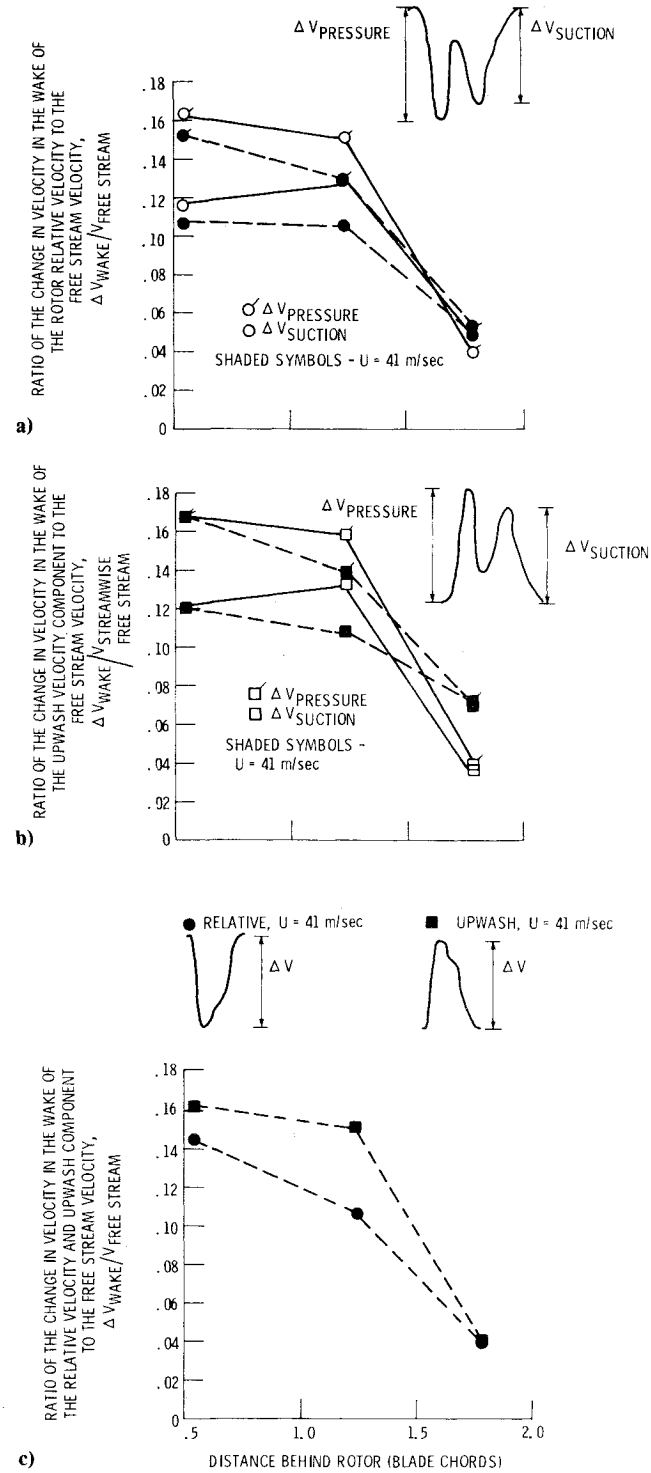

Fig. 7 Effect of downstream distance and forward velocity on the change in the velocity in the wake at 9.0% of the span from the tip. a) Rotor relative velocity, 80% of design rpm; b) upwash component, 80% of design rpm; c) rotor relative velocity and upwash component, 115% of design rpm.

Another parameter commonly used to describe the wake is the wake width. The wake width is measured at the point where the wake velocity is half of its extreme value. Figure 8 shows the effects of downstream distance and forward velocity on the wake widths which have been normalized by the spacing between blades. Because of the complex shapes of the wake waveforms near the blade tip, only the widths of the wakes at the station 30% of the span from the tip were measured. At 80% of design speed, the wake widths of both velocities gradually increase with increasing downstream

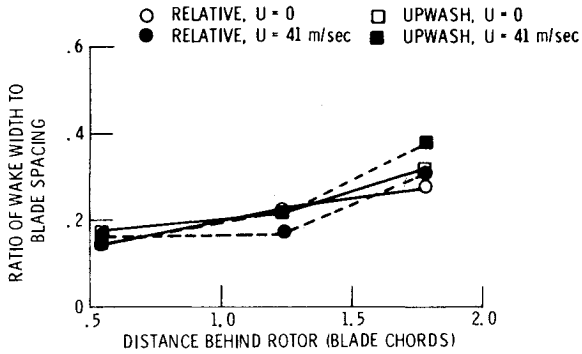

Fig. 8 Effect of downstream distance and forward velocity on the width of the rotor wake at 30% of the span from the tip, 80% of design rpm.

distance. The upwash component has a slightly higher wake width than the relative velocity. The effect of forward velocity is minimal.

Comparison of Mean Properties with Empirical Predictions

The effect of rotor wakes on aircraft engine compressor and turbine performance has been a concern for many years. Several empirical relationships developed by investigators have been widely used to predict the velocity defect in the wake. A summary of these empirical correlations is given by Dittmar.[15] Perhaps the prediction of velocity defect most often used was developed by Silverstein for an isolated airfoil in 1939.[16] The velocity defect is predicted to be

$$\frac{\Delta V_w}{V} = \frac{2.42\sqrt{C_D}}{(x/c+0.3)} \tag{1}$$

where ΔV_w is the maximum difference from freestream velocity in the wake; V is the freestream velocity; C_D is the profile drag coefficient; x is the downstream distance; and c is the rotor chord.

In 1953, Spence[17] fit his data for a turbulent wake behind an airfoil with

$$\frac{\Delta V_w}{V} = \frac{0.1265}{(x/c+0.025)^{1/2}} \tag{2}$$

From cascade investigations Lieblein and Roudebush[18] fit their data with

$$\frac{\Delta V_w}{V} = \frac{A_2\sqrt{C_D}}{(x/c+0.025)^{1/2}} \tag{3}$$

where

$$A_2\sqrt{C_D} = 0.13$$

In 1979, Reynolds and Lakshminarayana at Pennsylvania State University measured wake properties behind rotating blades with a triple wire anemometer.[19] Their velocity measurements of the defect of the relative velocity correlated well with the expression

$$\Delta V_w/V = C_D^{1/2}\,[B_5(s/c-s_o/c)^{-1/2} + B_6(s/c-s_o/c^{-1})] \tag{4}$$

where s is the streamwise distance, s_o is the streamwise virtual origin and B_5 and B_6 are constants for the far wake region where $s/c > 0.25$:

$$s_o/c = -0.36 \qquad B_5 = 0.271 \qquad B_6 = 0.0$$

In 1980, Ravindranath and Lakshminarayana performed a similar experiment behind a rotor with greater loading.[20]

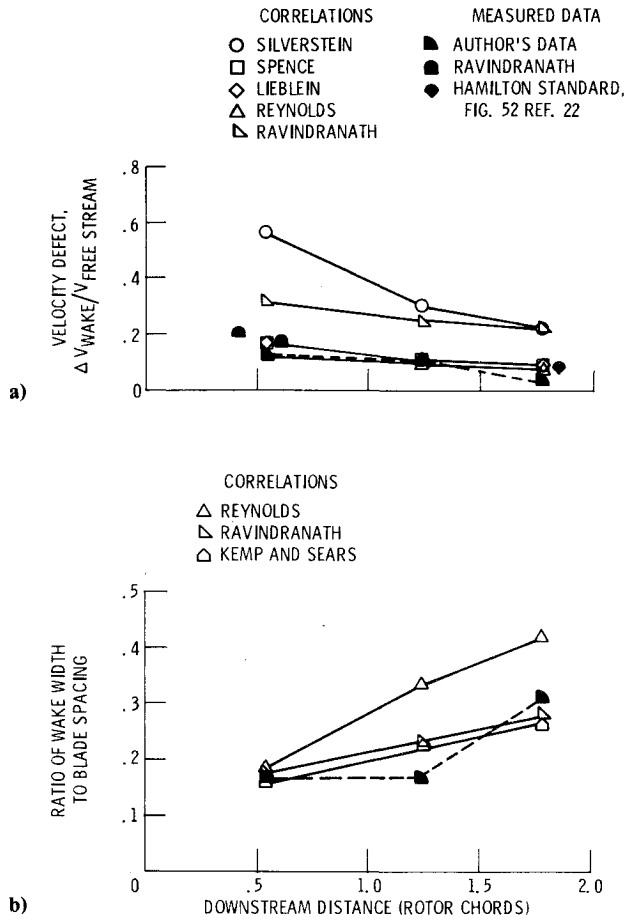

Fig. 9 a) Comparison of measured wake velocity defect in rotor relative system with correlations and other data, 30% of span from tip, 80% of fan design speed, $U = 41$ m/s. b) Comparison of measured wake width in rotor relative system with correlations and other data, 30% of span from tip, 80% of fan design speed, $U = 41$ m/s.

Their wake data in the axial direction correlated well with the following:

$$\Delta V_w/V = C_D^{1/2}\,[0.39\,(z/\cos\beta_o)^{-1} + 0.984] \tag{5}$$

for

$$0.2 < (z/\cos\beta_o) < 0.8$$

where z is the axial distance from blade trailing edge normalized by rotor blade chord and β_o is the blade outlet angle.

Figure 9a shows a comparison of the data measured in the present experiment with results predicted by these empirical equations. The empirical predictions were calculated using the profile drag coefficient approximated by Shepherd[21] to be

$$C_D = \frac{\bar{\omega}_p \cos^3\beta_\infty}{\sigma\cos^2\beta_1} \tag{6}$$

where σ stands for solidity; β_1 is the relative flow angle at rotor inlet; $\beta_\infty = \tan^{-1}\{\frac{1}{2}(\tan\beta_1 + \tan\beta_2)\}$; β_2 is the relative flow angle at rotor exit; and $\bar{\omega}_p$ is the profile loss coefficient. The values of the aerodynamic parameters used in this expression were obtained from Ref. 7 for a radial station 30% of the span from the tip at 80% of the fan design speed. Figure 9a indicates that the author's data agree well with the empirical correlations and Spence, Lieblein, and Reynolds. However, the correlations of Silverstein and Ravindranath overpredict the velocity defect. Although Silverstein's, Ravindranath's, and Lieblein's equations present the velocity defect to be a function of $C_D^{1/2}$ only Lieblein allows the con-

stant A_2 to vary with the drag coefficient. The best prediction of the velocity defect, however, is based on Reynolds correlation with $C_D^{1/2}$. It should be noted that the expressions developed by both Reynolds and Ravindranath have been extrapolated beyond the downstream limits of the data used to construct them in order to make a comparison with present data. Figure 9a also shows a comparison of the author's data with data measured by Ravindranath and Lakshminarayana[20] and Magliozzi et al.[22] at Hamilton Standard.

Ravindranath and Lakshminarayana measured data behind an experimental rotor with a design speed of 1066 rpm at an operating flow coefficient (relative velocity/tip velocity) of 0.56. The data measured by Magliozzi et al. were taken behind a 12-bladed rotor with a pressure ratio of 1.07 at a rotor speed of 6620 rpm. Although both sets of measured velocity defects are greater than measured in the present experiment, the measured 9×15-ft tunnel data does follow the trend of the other experimental results.

A comparison of the author's measured wake widths with those predicted by correlations of Kemp and Sears, Reynolds and Lakshiminarayana, and Ravindranath and Lakshminarayana is presented in Fig. 9b.

In the far wake, Reynolds and Lakshiminarayana[19] predict the wake width normalized by the blade spacing (δ/s_p) to be

$$\delta/s_p = C_D^{1/2}\,[0.735\,(s/c - 0.258)^{1/2}] \tag{7}$$

Ravindranath and Lakshminarayana[20] correlated their data in the far wake with

$$\delta/s_p = 0.5\sqrt{C_D}\,[0.833\,(z/\cos\beta_o) + 1.302] \tag{8}$$

In Ref. 23 Kemp and Sears used the following modified form of the wake width equation developed by Silverstein et al.,[16]

$$Y = 0.68\sqrt{2C_D^{1/2}}\,c_h\,(x/c_h - 0.7)^{1/2} \tag{9}$$

where Y is the half-width of the viscous wake; c_h is the airfoil half-chord; and x is the distance along airfoil measured from midchord.

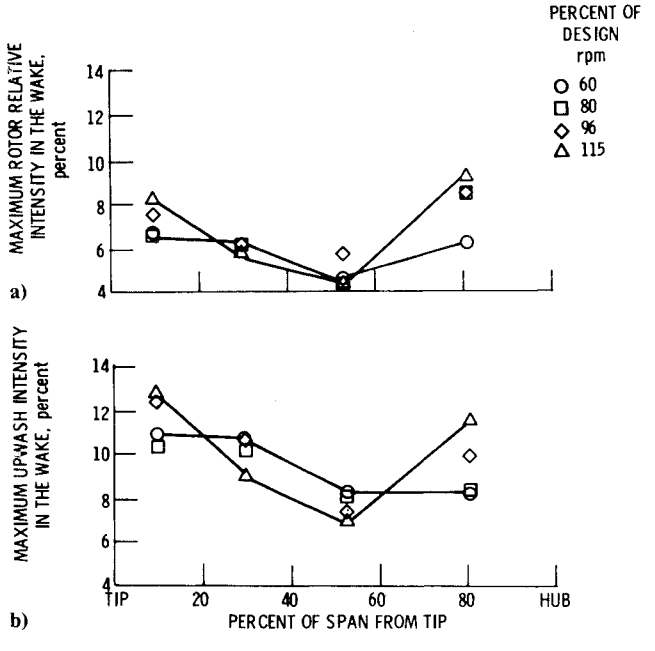

Fig. 10 Radial variation of the maximum intensity in the wake, 0.54 chord spacing, $U = 41$ m/s. a) Rotor relative intensity; b) upwash intensity.

The data in Fig. 9b agree well with the empirical correlations at the closest spacing but does not show the constant rate of increase that the correlations predict.

Since the empirical wake models repeated in Refs. 16-20 do not incorporate any analysis of the secondary flow phenomena affecting the wakes in the tip and hub regions of the fan, data comparisons with these models were made only in the midspan region. It is beyond the scope of this paper to form a general wake model describing the complicated wake pattern observed in the tip and hub regions.

Wake Turbulence Properties

The influence of the acoustic field in the fan duct on the turbulence levels measured by the anemometer were of some concern. The method outlined by Ko and Ho in Ref. 24 was used to estimate the ratio of the component of the cross-film signal associated with turbulent or unsteady aerodynamic fluctuations to the acoustic component estimated from pressure levels measured by a wall microphone located ahead of the rotor. The ratio at blade passing frequency was 16 dB, indicating that the anemometer signal was controlled by the unsteady aerodynamic flowfield rather than the acoustic field.

The effects of fan speed on the maximum turbulence intensity levels in the wake at the close rotor stator spacing with a forward velocity of 41 m/s are shown in Fig. 10. The levels of intensity in the wake are higher for the upwash (Fig. 10b) compared to the intensity measured for the relative velocity (Fig. 10a). The fluctuating upwash and relative velocities were normalized by streamwise and relative freestream mean velocities, respectively. In general, away from the hub and tip measuring stations, an increase in fan rotational speed was accompanied by a decrease in turbulence intensity level. This same trend was observed by Lakshminarayana et al. for the relative tangential and axial velocity components in Ref. 11. In the near tip and hub regions, however, an increase in fan

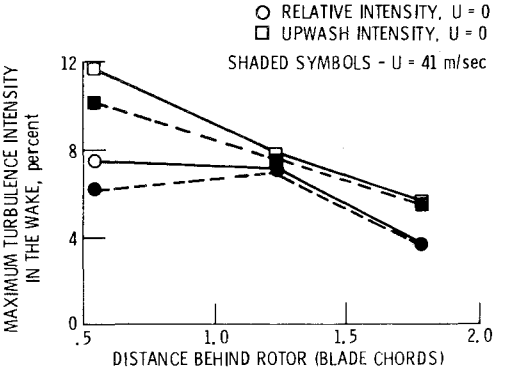

Fig. 11 Effect of downstream distance and forward velocity on the maximum relative and upwash turbulence intensity in the wake at 30% of span from the tip, 80% of design rpm.

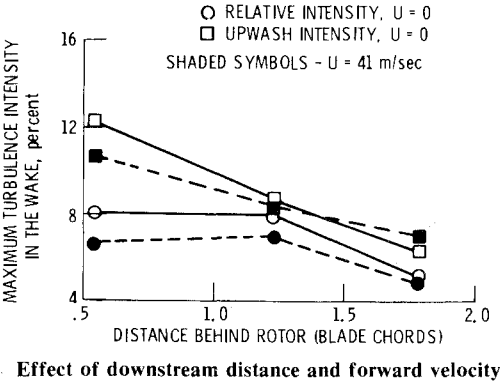

Fig. 12 Effect of downstream distance and forward velocity on the maximum relative and upwash turbulence intensity in the wake at 9% of span from the tip, 80% of design rpm.

rotational speed from 60 to 115% of design speed brought a definite increase in the turbulence intensity levels of both components at the closest rotor-stator spacing. These high intensity levels occur in regions where the measured aerodynamic losses are high[7] and secondary flows are prominent.

Figures 11 and 12 present the effects of downstream distance and forward velocity on the maximum levels of the upwash and relative turbulence intensities in the wake at 80% of design rpm. To study the effects of forward velocity, that is, a reduced level of fan inflow disturbances including turbulence,[13] wake turbulence intensities are presented with both forward velocity ($U=41$ m/s) and static tunnel operating conditions ($U=0$).

At a probe immersion of 30% of the span from the tip, it can be seen from Fig. 11 that the maximum intensity of the upwash component is at a higher level than that of the relative velocity. Forward velocity, which reduces the level of the turbulence to the rotor, also reduces the maximum wake turbulence level at the 0.54-chord rotor-stator spacing. The decay rate for the upwash component between the first two downstream measuring stations is slightly greater for the static tunnel operating condition (high inflow turbulence) than for the forward velocity conditions. This trend is in agreement with Hah and Lakshminarayana's findings that the maximum turbulence intensity increases with an increase in freestream turbulence level, but decays faster at higher values of freestream turbulence intensity.[14] As can be seen in Fig. 11, there is little decay, even a slight increase in the rotor relative intensity between the first two downstream measuring stations.

In the tip region of the blades (Fig. 12) at 80% of design speed, the turbulence intensity levels for both the upwash and rotor relative velocities are slightly higher than they are at a probe immersion of 30% of the span (Fig. 11). The decay rates of intensity for the two probe immersions are similar.

Spectral Analysis of Rotor Wakes

The ensemble averaged waveforms were analyzed by fast Fourier transform methods to determine their harmonic content. Data from this analysis are more descriptive of the waveform than parameters such as the wake defect and wake width, especially for the complicated wake profiles observed near the tip. In addition, in this form the data are probably more useful for analysis of the noise caused by the wakes impinging on the stators. There is a direct frequency correspondence between the harmonics of the wake and the harmonics of the sound field generated in the wake-stator interaction.[3]

Typical spectra of the ensemble averaged wake velocities are shown in Fig. 13. The figure shows the spectra of the rotor relative and upwash velocities at 1.23 rotor chords downstream at 80% of design speed and at a probe immersion of 30% of the span from the tip. The measured velocities were normalized to a reference velocity of 3.05 m/s and the spectra of the normalized velocity squared were computed in decibels.

Figures 14-16 utilize data from spectra such as these for the rotor relative and upwash velocities to examine the changes of spectral content with downstream distance and to compare the spectral content at two radial probe immersions all with a tunnel flow of 41 m/s.

Figure 14 shows the harmonic content of the upwash and rotor relative components of velocity at 80% of design speed at a probe immersion of 30% of the span from the tip. The rotor relative component increases slightly at the blade passage frequency (BPF) and its second harmonic ($2\times$BPF) between the first two downstream measuring stations while the third harmonic drops off slightly. At the closest rotor-stator spacing, the level of the BPF and its second and third harmonics are nearly the same. This same trend at the closest spacing is observed for the upwash component but at a slightly higher decibel level. The upwash component shows a

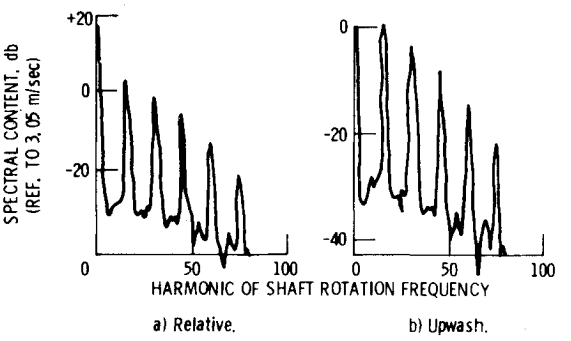

Fig. 13 Enhanced spectra of relative and upwash velocity at 80% of design rpm, 1.23 chord spacing, 30% of span from the tip, $U=41$ m/s.

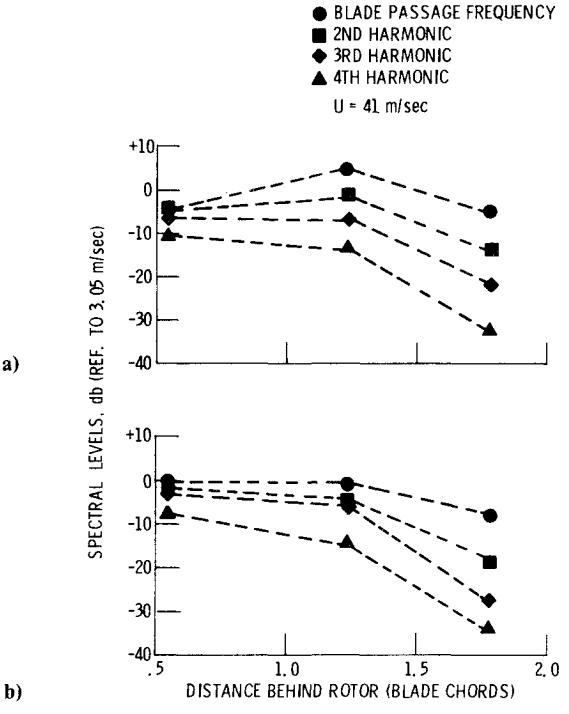

Fig. 14 Harmonic levels from ensemble averaged spectra, 30% of span from the tip, 80% of design rpm. a) Rotor relative velocity; b) upwash component.

nearly constant level at the blade passage frequency and its second harmonic between the first two downstream stations. In general, there is a sequential ordering of the harmonics of the blade passing frequency at all three downstream measuring stations for both velocity components.

In contrast to this sequential harmonic ordering at the 30% probe immersion, Fig. 15 indicates a nearly constant dominant level of the second harmonic between the first two downstream stations in the tip region at 80% of design rpm with a falloff at the blade passage frequency between these stations. The high levels of the second harmonic indicate the two oscillations in velocity for each blade gap which persist even to the farthest downstream measuring station (see sketches in Fig. 7).

Figure 16 shows that the levels at blade passage frequency and its harmonics decrease with increasing downstream distance for both the rotor relative and upwash velocities at 115% of design rpm at a near tip probe immersion. The blade passage frequency level is nearly 10 dB higher at the near tip immersion at 115% of design rpm compared to the 30% of span probe immersion. The effect of increasing fan rotational speed near the tip is to raise the level of the blade passage frequency and its harmonics. At the higher fan speed the amplitude of the blade passage frequency instead of its second

harmonic dominates the spectra at all three downstream positions. These high levels at the blade passage frequency are indicative of the waveforms sketched in Fig. 7c which show that the two regions of velocity change behind the blade caused by the blade wake and secondary flow effects have now merged. Not only is the blade passing frequency amplitude dominant at the tip region at the higher fan speed, but the harmonic levels of the blade passage frequency now follow a sequential ordering at all three downstream measuring stations.

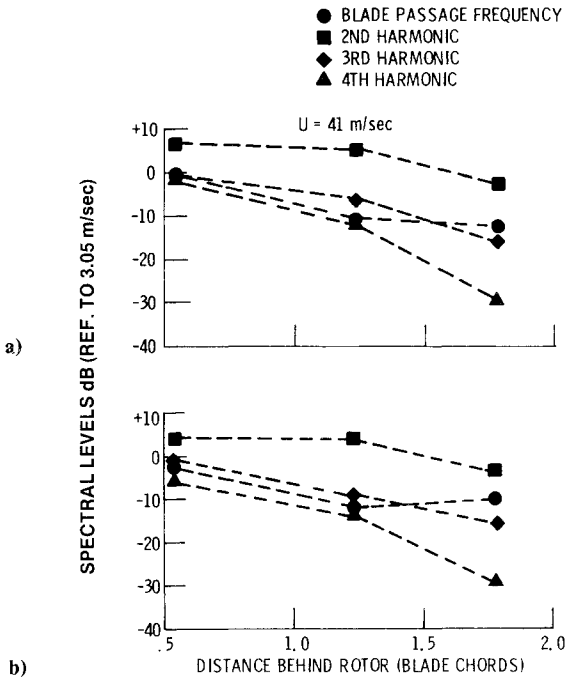

Fig. 15 Harmonic levels from ensemble averaged spectra, 9% of span from the tip, 80% of design rpm. a) Rotor relative velocity; b) upwash component.

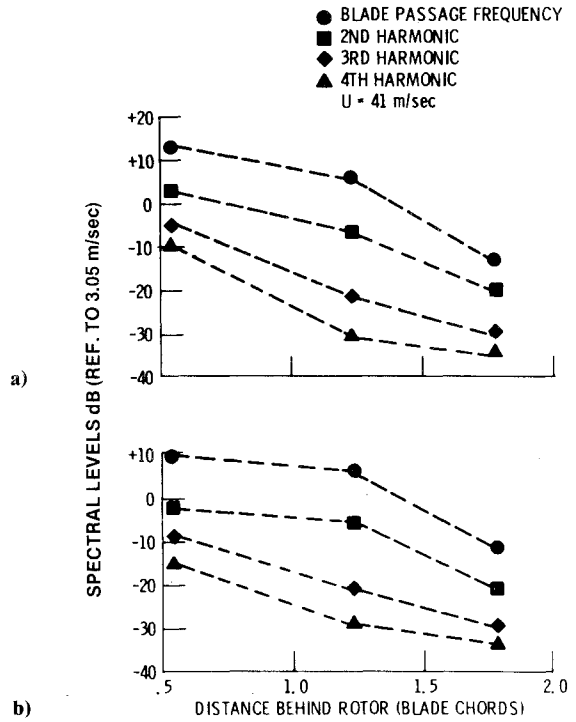

Fig. 16 Harmonic levels from ensemble averaged spectra, 9% of span from the tip, 115% of design rpm. a) Rotor relative velocity; b) upwash component.

A comparison of the trends of the harmonic content of the rotor wakes in the mid and tip regions of the duct and the harmonic content of the far-field acoustic signal is made in Ref. 3.

Summary of Results

An experiment was conducted to determine the mean and turbulence properties and the harmonic content of the blade wakes as a function of distance downstream of an aerodynamically loaded rotor. The effects of fan rotational speed and inflow turbulence were also studied.

The rotor wake mean velocities varied considerably in amplitude and width across the blade span from hub to tip. The mean wake waveforms near the tip are characterized by two regions of velocity change behind each blade at the lower fan speeds. These waveforms indicate that a velocity change due to the blade wake along with a velocity change due to a secondary flow phenomenon are present even at the farthest rotor-stator spacing. Above design speed only one wide wake in the tip region is observed, indicating that the blade wake and secondary flow effects have merged.

The normalized wake magnitude decreases with increasing downstream distance from the rotor. In general, forward velocity has an inconsistent but minimal effect on the wake magnitude. The wake magnitude decays at a faster rate as axial distance is increased beyond 1.2 rotor chords. An increase in fan speed causes a large increase in the wake magnitude parameter near the hub. The width of the rotor wake gradually increases with increasing axial distance.

The measured mean rotor wake defects agree well with the data measured by other experimenters and the correlation developed by Reynolds where the wake velocity defect is a function of $C_D^{1/2}$.

The maximum turbulence intensities in the wake for the relative and upwash velocities decrease with increasing downstream distance. Forward velocity decreases the maximum intensity levels in the wake for both velocities at the 0.54-chord measuring station. In general, an increase in the fan speed causes an increase in the maximum turbulence intensity levels near the hub and tip, but a decrease near the midspan region.

Although only two components of velocity were measured in the present experiment, the data presented in this paper provide insight into the complex nature of the velocity components of the rotor wakes. The determination of the harmonic content of the rotor wake velocity profiles provides a key ingredient required for the analysis of fan tone noise generated by rotor-stator interaction for this fan. Additional experiments and data analysis on other fans are needed in order to derive a consistent vortex and wake model reflective of spanwise variations. Such a model would permit parametric generation studies to determine the relative contributions of wakes and vortices to fan noise.

References

[1] Hanson, D.B., "Unified Analysis of Fan Stator Noise," *The Journal of the Acoustical Society of America*, Vol. 54, Dec. 1973, pp. 1571-1591.

[2] Dittmar, J.H., "Interaction of Rotor Tip Flow Irregularities with Stator Vanes as a Noise Source," NASA TM-73706, 1977.

[3] Woodward, R.P. and Glaser, F.W., "Effects of Blade-Vane Ratio and Rotor-Stator Spacing on Fan Noise with Forward Velocity," AIAA Paper 81-2032, Oct. 1981.

[4] Shaw, L.M. and Glaser, F.W., "Mean Rotor Wake Characteristics of an Aerodynamically Loaded 0.5 m Diameter Fan," NASA TM-81657, 1981.

[5] Yuska, J.A., Diedrich, J.H., and Clough, N., "Lewis 9- by 15-Foot V/STOL Wind Tunnel," NASA TM X-2305, 1971.

[6] Rentz, P.E., "Softwall Acoustical Characteristics and Measurement Capabilities of the NASA Lewis 9×15 Foot Low Speed Wind Tunnel," Bolt, Beranek, and Newman, Inc., Canoga Park, Calif. BBN-3176, June 1976; see also NASA CR-135026, June 1976.

[7] Lewis, G.W. Jr. and Tysl, E.R., "Overall and Blade-Element Performance of the 1.20-Pressure-Ratio Fan Stage at Design Blade Setting Angle," NASA TM X-3101, 1974.

[8] Abbott, J.M., Diedrich, J.H., and Williams, R.C., "Low-Speed Aerodynamic Performance of 50.8 Centimeter-Diameter Noise-Suppressing Inlets for the Quiet, Clean, Short-Haul Experimental Engine (QCSEE)," NASA TP-1178, 1978.

[9] Phillips, W.R.C. and Head, M.R., "Flow Visualization in the Tip Region of a Rotating Blade Row," *International Journal of Mechanical Science*, Vol. 22, 1980, pp. 495-521.

[10] Lakshminarayana, B. and Ravindranath, A., "Interaction of Compressor Rotor Blade Wake with Wall Boundary Layer/Vortex in the End-Wall Region," ASME Paper 81-Gr/GT-1, April 1981.

[11] Lakshminarayana, B., Govindan, T.R., and Reynolds, B., "Effects of Rotation and Blade Incidence on the Properties of the Turbomachinery Rotor Wake," AIAA Paper 81-0054, Jan. 1981.

[12] Heidmann, M.F. and Dietrich, D.A., "Simulation of Flight-Type Engine Fan Noise in the NASA Lewis 9 × 15 Anechoic Wind Tunnel," NASA TM X-73540, 1976.

[13] Shaw, L.M., Woodward, R.P., Glaser, F.W., and Dastoli, B.J., "Inlet Turbulence and Fan Noise Measured in an Anechoic Wind Tunnel and Statically with an Inlet Flow Control Device," NASA TM-73723, 1977.

[14] Hah, C. and Lakshminarayana, B., "Free Stream Turbulence Effects on the Development of a Rotor Wake," AIAA Paper 80-1431, July 1980.

[15] Dittmar, J.H., "Methods for Reducing Blade Passing Frequency Noise Generated by Rotor-Wake-Stator Interaction," NASA TM X-2669, 1972.

[16] Silverstein, A., Katzoff, S., and Bullivant, W.K., "Downwash and Wake Behind Plain and Flapped Airfoils," NACA TR-651, 1939.

[17] Spence, D.A., "Growth of the Turbulent Wake Close Behind an Airfoil at Incidence," Aeronautical Research Council, Great Britain, ARC-CP-125, 1953.

[18] Lieblein, S. and Roudebush, W.H., "Low-Speed Wake Characteristics of Two-Dimensional Cascade and Isolated Airfoil Sections," NACA TN-3771, 1956.

[19] Reynolds, B. and Lakshminarayana, B., "Characteristics of Lightly Loaded Fan Rotor Blade Wakes," NASA CR-3188, 1979.

[20] Ravindranath, A. and Lakshminarayana, B., "Three Dimensional Mean Flow and Turbulence Characteristics of the Near Wake of a Compressor Rotor Blade," Pennsylvania State University, University Park, Pa., PSU-TURBO-R-80-4, June 1980; see also NASA CR-159518, June 1980.

[21] Shepherd, D.G., *Principles of Turbomachinery*, Macmillan, New York, 1961.

[22] Magliozzi, B., Hanson, D.B., Johnson, B.W., and Metzger, F.B., "Noise and Wake Structure Measurements in a Subsonic Tip Speed Fan," NASA CR-2323, 1973.

[23] Kemp, N.H. and Sears, W.R., "The Unsteady Forces Due to Viscous Wakes in Turbomachines," *Journal of the Aeronautical Sciences*, Vol. 22, July 1955, pp. 478-483.

[24] Ko, W.M. and Ho, K.K., "Response of Hot Wire to Sound Pressure in an Airstream," *Transactions on Instrumentation and Measurement*, Vol. IM-23, Sept. 1974, pp. 211-214.